Chemistry–A European Journal
Research Article
doi.org/10.1002/chem.202300077
Chemistry Europe
European Chemical Societies Publishing
www.chemeurj.org

VIP Insight into the Structural and Emissive Behavior of a Three-Dimensional Americium(III) Formate Coordination Polymer

Aaron D. Nicholas,[a] Ana Arteaga,[a] Lucas C. Ducati,[b] Edgar C. Buck,[a] Jochen Autschbach,*[c] and Robert G. Surbella, III*[a]

Abstract: We report the structural, vibrational, and optical properties of americium formate ($Am(CHO_2)_3$) crystals synthesized via the in situ hydrolysis of dimethylformamide (DMF). The coordination polymer features Am^{3+} ions linked by formate ligands into a three-dimensional network that is isomorphous to several lanthanide analogs, (e.g., Eu^{3+}, Nd^{3+}, Tb^{3+}). Structure determination revealed a nine-coordinate Am^{3+} metal center that features a unique local C_{3v} symmetry. The metal–ligand bonding interactions were investigated by vibrational spectroscopy, natural localized molecular orbital calculations, and the quantum theory of atoms in molecules. The results paint a predominantly ionic bond picture and suggest the metal-oxygen bonds increase in strength from Nd–O < Eu–O < Am–O. The optical properties were probed using diffuse reflectance and photoluminescence spectroscopies. Notably, the rarely reported $^5D_{1'} \rightarrow {}^7F_{0'}$ emission band is observed and dominates the emission spectrum. This behavior is unusual and is attributed to the C_{3v} coordination environment of the metal center.

Introduction

A fundamental understanding of the transuranium elements, such as their electronic configuration and role of 5*f* orbitals in bonding, continues to be hampered by the lack of available compounds from which to establish periodic trends and quantify behavior. Scarcity of material and isotopes, as well as the radiological hazards associated with handling highly radioactive materials are the primary culprits. Chemical exploration of the element americium (Z = 95) in particular, suffers from this problem. This is highlighted by a recent search of the Cambridge Crystallographic Database, which contains over a million known crystal structures but only resulted in 55 known americium bearing compounds (Table S1, CSD version 2022.2.0).[1-31] For comparison, a search of uranium and plutonium resulted in 8,376 and 232 compounds, respectively. This problem is not unique to americium but in fact also exists for the other transuranium elements such as, curium–californium. Broadly, the lack of available data from which to extract trends across the actinide series limits our ability to predict chemical behavior and utilize these elements in future technologies. The obvious solution to this problem is to broaden and diversify the known examples of transuranium, and in particular of transplutonium, compounds.

Metal-organic frameworks (MOFs) consist of metal ions or clusters connected into two-dimensional (2-D) or three-dimensional (3-D) networks through organic ligands, and are an emerging viable route to probe the fundamental properties of actinides.[32,33] Such materials can be defined as a specialized subclass of coordination polymers that potentially contain solvent-accessible void spaces. Examples of transuranium metal-organic frameworks (TRU-MOFs) have recently begun to appear in the literature and in only the last four years are the actinides plutonium,[34] neptunium,[35,36] and americium[17] represented. For example, properties such as unusual local coordination and thermal stability, have been studied using these framework solids as hosts to immobilize actinides and study their behavior.

The first 3-D porous americium containing MOF was recently reported by Ridenour et al. utilizing the synthetic protocol for the rare earth containing GW-MOF6 series based upon adipic acid linkers.[17] The synthesis of Am-GW-MOF6 was accomplished by substituting the rare earth metal salt in favor of the actinide during preparation. The result was an isomor-

[a] A. D. Nicholas, A. Arteaga, E. C. Buck, R. G. Surbella, III
Pacific Northwest National Laboratory
902 Battelle Boulevard, Richland,
WA 99354 (USA)
E-mail: robert.surbella@pnnl.gov
[b] L. C. Ducati
Department of Fundamental Chemistry Institute of Chemistry
University of São Paulo
Av. Prof. Lineu Prestes 748, São Paulo,
05508-000 (Brazil)
[c] J. Autschbach
Department of Chemistry
University at Buffalo State University of New York
Buffalo, NY 14260-3000 (USA)
E-mail: jochena@buffalo.edu

Supporting information for this article is available on the WWW under https://doi.org/10.1002/chem.202300077

phous framework to the known lanthanide based MOF.[17,37,38] This resulting Am-MOF displayed evidence for weak guest-enhanced americium sensitization by organic molecules residing in the void spaces.

Carboxylic linkers such as adipic acid are particularly utilized in the formation of 3-D networks as the hard oxygen atoms readily coordinate with actinide metal ions, which typically exist in oxidation states greater than 3. The wide array of available organic linkers – and indeed known lanthanide MOFs – from which to rapidly synthesize families of TRU-MOFs is particularly attractive. Underlying this prospect, however, is the need for simple model compounds that can be used to interpret future findings within structurally and electronically complex TRU-MOFs.

Formate is the simplest form of a carboxylic acid. Formate ligands are capable of coordinating to metal ions in several motifs (Scheme 1) that are common to more complex carboxylic acids and may support assembly in one, two, and three dimensions. Because of the number of possible coordination modes, MOFs and coordination polymers experience significant differences in framework structure, void spacing, and metal–ligand bond strength. All of these factors are known to influence the resulting material properties.[39–43] The small size of the formate ion, however, prevents the formation of solvent accessible void spaces, reducing the complexity of the structure and properties associated with host-guest interactions. As such, compounds that utilize formate linkers represent the simplest type of a 3-D framework and may serve as a baseline model to interpret periodic trends and properties such as spectroscopic signatures.

Only a single instance of americium formate has been reported to date, by Weigel and Meer in 1967,[4] which was synthesized via the dissolution of americium hydroxide in concentrated formic acid. The initial report is limited to powder X-ray diffraction data which revealed that the structure was isomorphous with several analogous lanthanide formates as well as one uranium formate complex.[4,44–55] No optical or other spectroscopic properties were reported, and no further work has been published for this foundational complex. Therefore, we recognize the importance of completing the record with respect to the synthesis and interpretation of spectroscopic signatures.

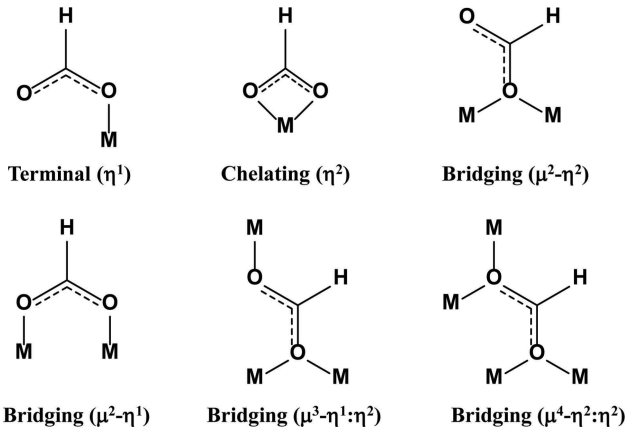

Scheme 1. Selected possible coordination modes of formate ions with metal centers.

Herein, we report the synthesis, structure, and optical properties of americium formate (**Am1**, $Am(CHO_2)_3$). This compound features Am^{3+} metal centers linked into a 3-D framework via formate ligands which are formed in situ by the hydrolysis of dimethylformamide solvent molecules. The nine-coordinate Am^{3+} assumes a C_{3v} symmetry and is isomorphous to its Nd^{3+} and Eu^{3+} analogs,[47,53,54] which have both been synthesized here using the same in situ method to aid in the interpretation of the structural and optical properties of the title compound. Monitoring the formate IR vibrational modes, we have been able to determine that the relative metal–oxygen bond strength proceeds as Am > Eu > Nd. The UV-vis-NIR absorption spectrum of **Am1** was determined via diffuse reflectance spectroscopy measurements, displaying sharp *f-f* transition bands. Most notably, luminescence measurements reveal that americium formate is an active emitter when irradiated with UV-vis light, primarily through direct excitation from the 5*f* shell. This compound displays atypical Am^{3+} emission behavior where the rarely observed $^5D_1$-$^7F_0$ transition is the dominant emission band. The vibrational and spectroscopic measurements were extended to the known lanthanide analogs to unravel differences in the metal-ligand bonding and distinct spectroscopic signatures.

Experimental Section

General: *CAUTION:* ^{243}Am ($t_{1/2}$ = 7,370 years) is an α-particle and γ-radiation (142 keV) emitting radionuclide with high specific-activity (0.2 Ci g^{-1}) and hazardous α, β, and γ emitting daughters, (e.g., ^{239}Np with a $t_{1/2}$ = 2.35 days and a 278 keV γ-ray). ^{243}Am poses a serious health risk if not handled properly. All experiments with this isotope were performed within a specialized facility designed and designated for the handling of transuranium radionuclides. Synthesis and bulk crystal growth were conducted in a negative pressure radiological glovebox while individual samples were prepared for analysis in a radiological fume hood. Nitric acid (65% w/w HNO_3), benzene-1,3,5-tricarboxylic acid (BTC), $EuCl_3 \cdot 6H_2O$, and Nd_2O_3 were purchased from Millipore Sigma. Dimethylformamide (DMF) was purchased from ACROS Organics.

Synthesis: *$Am(CHO_2)_3$*, (**Am1**). 100 μL of a 66.3 mM $Am(NO_3)_3 \cdot xH_2O$ (1.61 mg Am^{3+}) stock solution in concentrated HNO_3 was transferred to a 3 mL PFA Savillex vial containing 180 μL di H_2O, 650 μL DMF, 5 μL concentrated HNO_3. The Savillex vial was sealed and placed into a furnace and heated to 75 °C for 72 h. The solution was allowed to cool to room temperature where large, pale orange, rod crystals formed. The crystals were washed three times with fresh DMF and prepared for diffuse reflectance and vibrational spectroscopy measurements. Microcrystalline powders of **Am1** were synthesized using a similar method. Here, 0.70 μL of $Am(NO_3)_3 \cdot xH_2O$ (0.340 mg Am^{3+}) was transferred to a 3 mL PFA Savillex vial containing 100 μL of 15.5 mM BTC in DMF (0.00155 mmol), 180 μL of H_2O, 650 μL of DMF and 5 μL of HNO_3 (0.073 mmol, 65% w/w). The Savillex vial was sealed and placed into a furnace and heated at 75 °C for 72 h. The solution was cooled, and a white microcrystalline product formed. Phase identification of the microcrystalline sample was confirmed by PXRD, and this material was used for

scattering electron microscopy (SEM) and luminescence measurements.

$Eu(CHO_2)_3$, (**Eu1**). A total of 178.6 μL of 0.06 M $Eu(NO_3)_3 \cdot 6H_2O$ in concentrated HNO_3 (70.5 mg Eu^{3+}) solution was transferred to a 3 mL PFA Savillex vial containing 180 μL di H_2O, 650 μL DMF, 5 μL concentrated HNO_3. The Savillex vial was placed in a furnace and heated at 75 °C for 72 h. Small, colorless, square crystals formed. Crystals were washed three times with fresh DMF.

$Nd(CHO_2)_3$, (**Nd1**). A total of 178.6 μL of 160 mM Nd_2O_3 in concentrated HNO_3 (99 mg Nd^{3+}) solution was transferred to a 3 mL PFA Savillex vial containing 180 μL di H_2O, 650 μL DMF, 5 μL concentrated HNO_3. The Savillex vial was placed in a furnace and heated at 75 °C for 72 h. Large, pale blue, tubular rod crystals formed. Crystals were washed three times with fresh DMF.

X-ray crystallography: Single crystals of **Am1**, **Eu1**, and **Nd1** were harvested from the mother liquor and mounted on 20 μm MiTeGen™ micromounts. Data were collected using monochromated Ag Kα (=0.56087) radiation on a Bruker D8 Venture, equipped with a Photon III CMOS detector. All reflection data were collected at 100(2) K or 298(2) K using 0.5° ϕ and ω scans. The data were reduced using SAINT[56] and an empirical absorption correction applied using SADABS,[57] all within the APEX3 software suite.[58] Structure solution was performed using direct methods (ShelXS) while subsequent refinements were performed using WinGX.[59] The heteroatoms were refined anisotropically while the aromatic hydrogen atoms were placed in idealized positions (AFIX43) and allowed to ride on the coordinates of the parent atom with isotropic thermal parameters (U_{iso}) fixed at 1.2 U_{eq}. Details of the X-ray diffraction experiments, and crystallographic data are summarized in Table 1. Thermal ellipsoidal plots were rendered using ORTEP[60] and select bond lengths and bond angles can be found in the Supporting Information, Figures S1-S4. Details of crystallographic refinement can also be found in the Supporting Information.

Photophysical Measurements: Diffuse reflectance spectra were collected on bulk solid samples of **Am1**, **Eu1**, and **Nd1** at 298 K. The light source was a Mikropack DH-2000-BAL deuterium and halogen light source coupled with an Ocean Optics Flame detector. Scattered light was collected with a fiber-optic cable. Spectra were referenced with barium sulfate ($BaSO_4$). Data were processed using OceanView spectroscopy software. Steady-state luminescence scans were collected at 298 K. Spectra were collected with a Nano-log®-3 photoluminescence spectrophotometer from Horiba using a 450 W xenon arc lamp combined with a double excitation monochromator and double emission monochromator. A photomultiplier tube at 950 V was used as the emission detector. Samples were mounted on a black mount using non-emitting high vacuum grease and sealed under a quartz plate.

Table 1. Crystal and structure refinement data.[a]

	Am1	Am1
Formula	$Am(CHO_2)_3$	$Am(CHO_2)_3$
Formula weight	376.11	376.11
Temp., K	298(2)	100(2)
Crystal System	Trigonal	Trigonal
Space group	R3*m*	R3*m*
Z	3	3
a/b, Å	10.614(2)	10.572(2)
c, Å	4.058(2)	4.045(2)
α/β, °	90	90
γ, °	120	120
Volume, Å^3	395.9(2)	391.5(2)
ϱcalc, g cm^{-3}	4.757	4.786
μ, mm^{-1}	14.497	14.661
Radiation	Ag Kα (0.56087 Å)	Ag Kα (0.56087 Å)
Residuals:[a] R_1; wR_2	0.0064; 0.0145	0.0095; 0.0228
Goodness of fit	1.203	1.137
CCDC no.	2161095	2161094

[a] $R_1 = \Sigma||F_o| - |F_c|| / \Sigma|F_o|$ for observed data only. $wR_2 = \{\Sigma[w(F_o^2 - F_c^2)^2] / \Sigma[w(F_o^2)^2]\}^{1/2}$ for all data.

Powder X-ray Diffraction: Dried microcrystalline powders of **Am1** were placed on a zero-background plate within a Bruker PXRD material holder (C79298A3244D97). Radiological samples were covered with Kapton film as primary containment. The bulk material was characterized using a Rigaku Ultima IV diffractometer (Cu-Kα radiation). The scans were collected using 5 mm divergence slit, 0.5 mm incident slit, receiving 5° side solar slits, and a Ni foil filter (to reduce contributions from Kβ). The data were collected in 0.02° count binning steps at a scan rate of 0.5° min^{-1}, from 5–90° 2θ, Figure S5. PXRD data indicates a common unknown impurity (unexpected peak at 18.1° 2θ) in **Am1** samples prepared via both synthetic routes.

Scanning Electron Microscopy and Energy Dispersion Spectroscopy (SEM-EDS): Images of **Am1** were collected on a FEI (ThermoFisher Hillsboro, OR) Quanta 250FEG Scanning Electron Microscope between 5 and 25 keV under low vacuum using a backscattered electron detector. Compositional analysis was determined using an Octane Elect silicon drift detector from EDAX (EDAX Inc., Mahwah, NJ) X-ray energy dispersive spectroscopy (EDS) system using GENESIS acquisition software. The spectra were modeled using DTSA II (Microscopium), Figure S6.[61]

Vibrational Spectroscopy: "Spectroscopic measurements were performed on single crystals of Am1, Eu1, and Nd1 at 298 K using a Bruker Lumos Fourier-transform infrared spectrometer (FTIR) with an attenuated total reflection accessory. This instrument is equipped with a digital charge coupled device camera. Sixty-four individual measurements were collected on three to five individual crystals from each sample. Data were collected between 600 cm^{-1} and 4,000 cm^{-1} with a resolution of 4 cm^{-1} and analyzed using the OPUS V.7.2 software."

Computational Details: Inner sphere bonding was investigated using the QTAIM and Natural Bond Orbital (NBO) based Natural Localized Molecular Orbital (NLMO) methods to understand and rationalize covalency as well as atomic orbital hybridization and involvement. Models, monomeric and dimeric, were built from crystallographic subunits in their experimental structures and used without optimization. Rendered models can be found in the Supporting Information (Figure S10–S11). Calculations were performed within the Amsterdam Density Functional (ADF) program[62] using the scalar relativistic zeroth-order regular approximation Hamiltonian, the M06-2X DFT-KS functional, and an all-electron triple-zeta doubly polarized Slater-type basis set. Calculations were performed with a single spin multiplicity (Nd = f3, quartet; Eu/Am = f6, septet). The NLMO analysis was obtained with the NBO program v6.0 included in the ADF package.[63] Only data for the alpha spin NLMOs are reported herein. QTAIM utilized the corresponding module implemented in ADF. NLMO and QTAIM parameter values for the monomeric models were consistent with those of the dimeric models. As such, we have opted to report just the dimeric values in the following discussion. Monomeric values can be found in the Supporting Information.

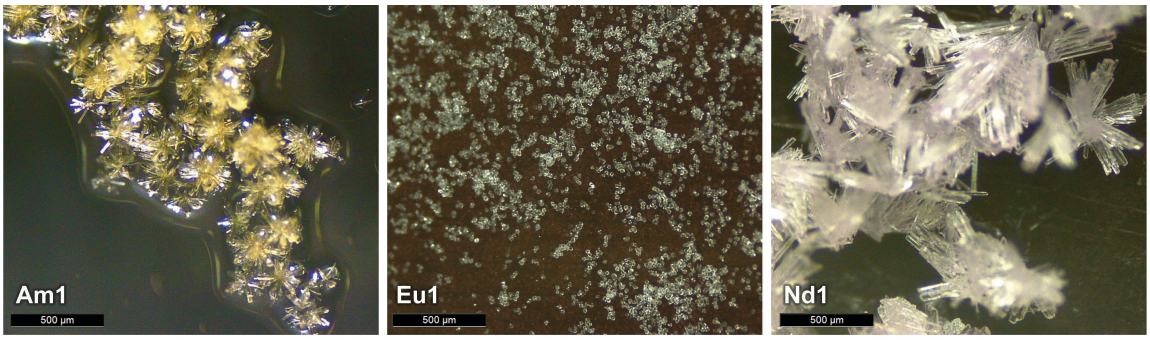

Figure 1. Photoimages of **Am1**, **Eu1**, and **Nd1** under microscope magnification (x5).

Table 2. Selected metal-oxygen distances of **Am1** in comparison with **Nd1** and **Eu1** at 298 K.

Bond	Bond lengths [Å] Am	Nd	Eu
M–O1 (η^1)	2.464(5)	2.4683(18)	2.416(5)
M–O2 (η^2)	2.555(5)	2.5513(18)	2.505(6)
M–O2′ (η^2)	2.561(5)	2.5690(18)	2.536(6)

Results and Discussion

Synthesis

The compound **Am1** was synthesized from an acidic solution of americium nitrate in a mixture of DMF and deionized water. In situ hydrolysis of DMF in the presence of acid and heat resulted in the formation of formic acid and dimethylamine products, the former coordinating to the actinide ions.[64] The result was the formation of small pale orange rod-like crystals that were suitable for single crystal X-ray diffraction, Figure 1. Alternatively, microcrystalline powders can also be prepared from a similar solution that contains solvated BTC ligands (Figure S6) in which the formate ions outcompete the larger carboxylic acid for coordination. The BTC free in situ preparation was used successfully to produce large single crystals of the previously reported lanthanide analogs **Nd1** and **Eu1**.[47,53,54] The Nd^{3+} and Eu^{3+} containing compounds were used to rationalize the structural and spectroscopic data of the title compound. The Nd^{3+} ion in a nine-coordinate geometry has a radius of 1.163 Å, similar to Am^{3+} at 1.162 Å, and as such provides a suitable structural comparison.[65,66] Similarly, Eu^{3+} as a $4f^6$ ion shares a closely related electronic configuration to Am^{3+} ($5f^6$), and as such, serves as an spectroscopic surrogate for the heavier actinide.

Structure

The isomorphs **Am1**, **Eu1**, and **Nd1** crystallize in the trigonal space group *R*3 *m* and have nearly identical unit cell parameters (Table S2). As a representative structure, **Am1** features an asymmetric unit that contains a single crystallographically unique metal center and formate ligand. The Am^{3+} ion is coordinated by nine formate ligands to form a tricapped trigonal prismatic geometry, Figure 2. The formate ion assumes a bridging μ^3-η^1:η^2 coordination mode between three metal centers (Figure S7). The measured Am–O distances are 2.464(5) Å (Am1-O1 (η^1)), 2.555(5) Å (Am1-O2 (η^2)), and 2.561(5) Å (Am1-O2′ (η^2)). The metal center adapts a local C_{3v} symmetry due to the asymmetry of the Am–O contacts, Figure S8 and S9, which is unique among known Am^{3+} bearing compounds. This symmetry is preserved in **Nd1** and **Eu1** with a comparison of M–O distances in Table 2. Given the similarity in ionic radii, the compounds unsurprisingly show similar metal-ligand distances. Notably, however, the η^2 Am–O distances are slightly shortened (up to 0.23% in the case of O2′) compared to the analogous Nd–O distances whereas the η^1 bonds are essentially the same. The Eu–O distances are significantly shorter.

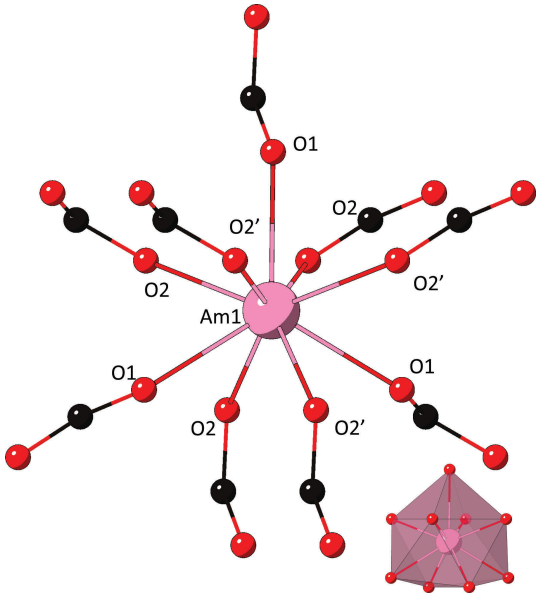

Figure 2. Local coordination geometry about the metal center in **Am1** with inset polyhedral representation of the inner coordination sphere. Color scheme: Am, pink; O, red; and C, black.

The global connectivity of **Am1** features bridging η^2 formate oxygens (O2/O2′) that link adjacent metal centers together, forming chains along the crystallographic *c*-axis. The chains are

in turn linked into a 3-D framework via the η^1 formate oxygen (O1), Figure 3. The η^2 coordination mode at the O2/O2′ atoms provides an explanation to the distance elongation for these atoms in comparison to the η^1 O1 atoms. The small size of the formate ion prevents formation of solvent accessible void spaces along the *c*-axis. The lack of solvent accessibility is important considering sensitization of Am^{3+} luminescence by light-harvesting guest molecules has been demonstrated in the other example of an Am MOF.[17] As such, the absence of guest molecules makes **Am1** an attractive control model in which to compare future TRU-MOF chemical behaviors as complex electronic pathways between linkers and/or guest molecules is limited.

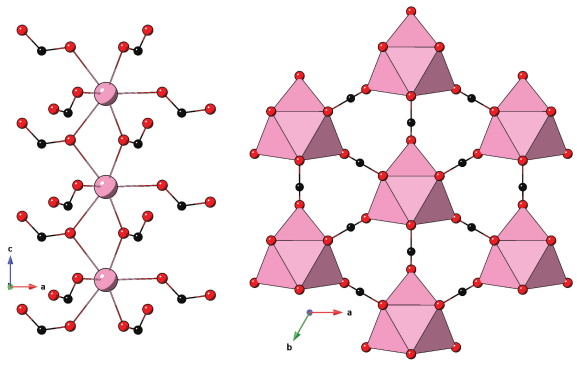

Figure 3. Left: A ball-and-stick representation of **Am1** (left) shows the chains that form along the *c*-axis by η^2 coordination of the formate ligands. Right: A polyhedral representation of **Am-1** highlights the 3.37(1) Å x 4.105(9) Å channels that propagate along the *c*-axis.

Vibrational Spectroscopy

The vibrational spectrum of **Am1** was collected alongside the **Eu1** and **Nd1** analogs to explore the involvement of the 5*f* shell in bonding. Results are shown in Figure 4 and summarized in Table 3. Formate has several IR active vibrational modes that may be influenced by coordination at either (or both) oxygen atoms.[67] The C–O stretch is particularly sensitive to changes in coordination mode and electron donation by the terminal O, marking it as an important spectroscopic probe for metal-O (M–O) bond analysis. For example, in aqueous solutions the symmetric C–O stretch occurs at 1,585 cm^{-1} whereas for solid Na_2CHO_2 this mode is shifted to 1,567 cm^{-1}. The asymmetric C–O stretch also shifts from 1,351 cm^{-1} in solution to 1,366 in Na_2CHO_2.[67] For **Am1** the symmetric and asymmetric C–O stretches are observed at 1,560 cm^{-1} and 1,309 cm^{-1}, respectively. The C–O stretch modes are progressively shifted to higher frequency for the **Eu1** and **Nd1** analogs to 1,312 cm^{-1} and 1,317 cm^{-1} for the symmetric and 1,562 cm^{-1} and 1,566 cm^{-1} for the asymmetric stretch, respectively. Plotting the frequencies versus the van der Waals (vdW) radii of Am, Eu, and Nd at 2.83 Å, 2.87 Å, and 2.95 Å, respectively, as suggested by

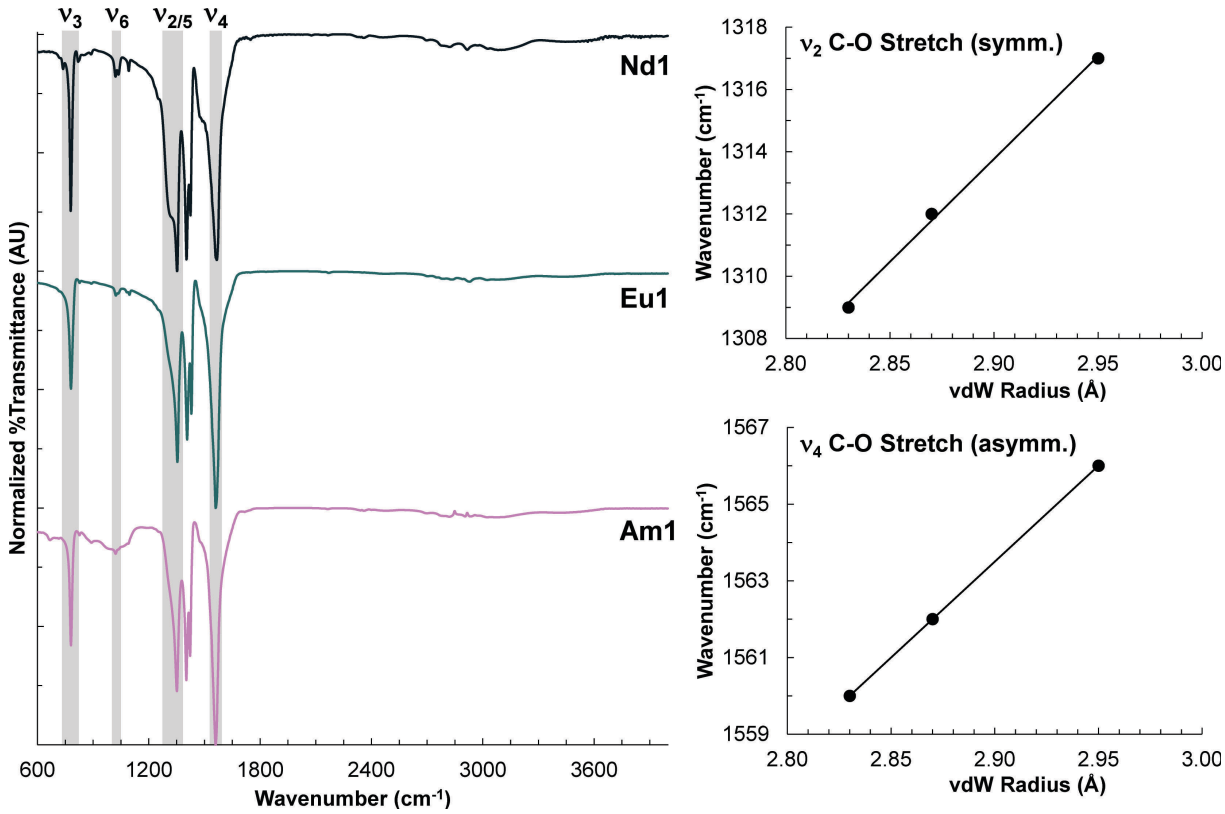

Figure 4. Left-to-Right: The FTIR spectra of **Am1**, **Eu1**, and **Nd1** and the plots of $\nu_{2/4}$ C–O stretch frequencies versus metal van der Waals radii. The IR active formate bands are highlighted in gray and normal modes labeled.

Table 3. Summary of the vibrational (IR) spectroscopy results for **Am1**, **Eu1**, and **Nd1**.[67]

	Am1	Eu1	Nd1
ν_2 C–O stretching (asymm) [cm^{-1}]	1309	1312	1317
ν_3 COO deformation [cm^{-1}]	781	781	779
ν_4 C–O stretching (symm.) [cm^{-1}]	1560	1562	1566
ν_5 COO rocking [cm^{-1}] (C–H bending, in-plane) [cm^{-1}]	1352	1354	1352
ν_6 COO rocking (C–H bending, out-of-plane) [cm^{-1}]	1024	1026	1022

Alvarez[68] and generally with ionic radii by Shannon (CN = 8)[65] reveals a linear relationship where the larger radii trend towards higher frequencies, and thus stronger C–O bonding. For formate, the highest occupied molecular orbital is a delocalized O–C-O π involving the unhybridized p_z C and O atomic orbitals.[69] As such, we expect increases in M–O bonding and accompanying backbonding to cause a decrease in the C–O vibrational frequency analogous to the metal-carbonyl interactions in organometallic complexes.[70,71] Based on the C–O frequencies in our formate series the M–O interaction strength is in the order **Am1** > **Eu1** > **Nd1**.

Computational Modelling

Experimental results and their implication on inner sphere bonding were substantiated by QTAIM and NBO calculations. Herein, our goal was to (1) evaluate the bond of the coordinated formate ligand (i.e., relative strengths, covalency, etc.) and (2) deduce the hybridization and identity of atomic orbitals involved as a function of metal. The QTAIM results for dimeric models are summarized in Table 4 for which the bond critical point (BCP) parameters around the metal atom are reported. For the formate compounds and the metal-oxygen interactions, the calculated electron density (ϱ) is <0.05 au, ranging between 0.047 au (**Am1**) and 0.036 (**Nd1**) and the Laplacian ($\nabla^2\varrho$) is >0 au. Typically, for a clear-cut covalent bond, $\varrho > 0.2$ and $\nabla^2\varrho < 0$. Therefore, both values indicate that the metal-ligand bonding in the present systems is dominated by non-covalent (ionic) interactions.[72] However, it has been noted repeatedly (e.g., recently in Ref. [73]), that QTAIM does not readily identify minor but important covalent components in actinide-ligand bonding. For example, the electron density is marginally largest in **Am1**, viz. 6–9% larger compared to the lanthanide analogs. Here, ϱ is largest for the η^1 O1 bond and smallest for the η^2 O2 bond, representing the strongest and weakest bonds, respectively. Overall, ϱ decreases in the order of **Am1** > **Eu1** > **Nd1** and is therefore consistent with the FTIR analysis. The mostly ionic nature of the metal-formate bond is further indicated by the generally positive values of the total energy densities (*H*). Both **Am1** and **Nd1** feature negative *H* values, yet the magnitude is nearly zero in each case. Despite the clear indication that the metal-formate bond is strongly ionic, according to the QTAIM metrics, we bring attention to the bond ellipticity parameters (ε) of **Am1**. These values are significantly smaller in **Am1** compared to analogous lanthanide BCP values. At a fundamental level the ellipticity describes the bond cylindrical symmetry where for formal single and triple bonds $\varepsilon = 0$ and double bonds $\varepsilon > 0$, (e.g., 0.000 for ethane vs. 0.330 for ethene).[74] The small ε values of **Am1** thus indicate the Am–O bond is single with a bond order of one .[75]

Evaluating formate hybridization and orbital involvement is the next step in understanding inner sphere coordination. For a free formate anion, the electronic structure according to an NBO/NLMO analysis is as follows: The C–H σ bond orbital and the two equivalent C–O σ bond orbitals involve the expected sp^2 hybrid atomic orbitals on the carbon. For each oxygen, one of the two lone pairs (LPs) is generated as an in-plane s-rich (62%) σ LP. The other one is generated as an in-plane 2p atomic orbital. The two in-plane 2p LPs of formate show considerable delocalization within the σ framework of orbitals, as indicated by the parent NBO occupations of only 1.86. For

Table 4. QTAIM topology parameters (atomic units) for the M–O and M–M bond critical points in **Am1**, **Eu1**, and **Nd1** dimeric models. Electron density, ϱ; Laplacian of the electron density, $\nabla^2\varrho$; ellipticity, ε; total energy density, H; potential energy density, V; kinetic energy density, G.

	Bond	ϱ	$\nabla^2\varrho$	ε	*H*	*V*	*G*	$\lvert V\rvert/G$
	Am–O1	0.04717	0.22231	0.00927	0.00085	−0.05388	0.05473	0.98452
Am1	Am–O2	0.03814	0.18595	0.00026	0.00309	−0.04031	0.04340	0.92888
	Am–O2′	0.03987	0.17591	0.01851	0.00130	−0.04138	0.04268	0.96951
	Am-Am	0.00975	0.04553	-0.84174	0.00252	−0.00635	0.00887	0.71613
	Eu–O1	0.04674	0.20912	0.03037	0.00001	−0.05225	0.05227	0.99975
Eu1	Eu–O2	0.03667	0.17042	0.01819	0.00258	−0.03745	0.04003	0.93556
	Eu–O2′	0.03729	0.15298	0.02227	0.00080	−0.03665	0.03745	0.97871
	Eu-Eu	0.00987	0.04916	−0.85726	0.00279	−0.00670	0.00950	0.70582
	Nd–O1	0.04576	0.18958	0.01959	−0.00101	−0.04942	0.04841	1.02092
Nd1	Nd–O2	0.03588	0.16097	0.02837	0.07513	−0.03582	0.03803	0.94190
	Nd–O2′	0.03766	0.14645	0.00894	0.00006	−0.03650	0.03656	0.99847
	Nd-Nd	0.00895	0.04388	-0.00862	0.00255	−0.00587	0.00842	0.69731

comparison, the two oxygen σ LPs have parent NBO occupations of 1.99, close to the idealized 2.00 for a perfectly localized Lewis-type orbital. The delocalized π system of free formate is in the NBO/NLMO analysis represented by one C–O π bond on one side, accompanied by a strongly delocalized oxygen 2p π lone pair on the other side with a parent NBO occupation of only 1.61. Together, the π bond and the delocalized π LP represent the 3-center-4-electron π bond of carboxylate. Donation (dative bonding) from the formate ligand to the metal may then take place via σ donation from the σ and in-plane 2p LPs, and via π donation from the occupied formate π framework. Given that the ligand has empty low-energy π* orbitals, there is also a possibility for π back-donation.

The metal-ligand bonding in **Am1** involves primarily the s-rich σ LPs of the oxygens. Representative examples are shown in Figure 5. In keeping with the mostly ionic bonding in the complex, the donation bonds in the system are strongly polarized toward the oxygens and indicate only minor involvement of the Am 5f and 6d shells, with at most a few weight-% of the orbital densities on Am (see Supporting Information). Representative atomic orbital renderings are shown in Figure 5.

In **Am1** the Am–Am distance of 4.058(2) Å represents 71.7% of the sum of the vdW (ΣvdW). While far outside the distance (3.451 Å–3.468 Å) for Am metal,[76] the short Am–Am distances in **Am1** give rise to the possibility of orbital interactions between actinide metal centers. Actinide-actinide bonding has so far largely been restricted to gas phase molecules or computationally predicted structures.[77–83] Two notable examples are a $\{Th(\eta_8\text{-}C_8H_8)(\mu_3\text{-}Cl)_2\}_3$ cluster complex by Liddle et al.[84] and a $U_2@C_{60}$ cage by Chen et al.[83] For $\{Th(\eta_8\text{-}C_8H_8)(\mu_3\text{-}Cl)_2\}_3$ Th–Th bonding occurs between the Th 6d orbitals whereas in the $U_2@C_{60}$ cage, the U–U bonds occur primarily between the U 5f orbitals.[84] The metal-metal bonding in these systems follows computational predictions where 5f orbital participation becomes more prevalent in the actinides following Th. With this in mind, we set out to determine the presence and nature of Am–Am bonding (if any).

Interestingly, both the QTAIM analysis and the NLMO analysis indicate the possibility of Am–Am orbital interactions. In QTAIM, there is a BCP identified between the Am^{3+} centers in **Am1** revealing electron density values similar to those found in the systems of **Eu1** and **Nd1**. These metal-metal BCPs, unlike those for the coordinated O atoms, are cage critical points and thus represent a local electron density minimum which increases in all three directions. The QTAIM parameters indicate the presence of electron density between each metal center (in **Am1**, **Eu1**, and **Nd1**), which trends with the short crystallographically oberseved metal–metal distances.[85] QTAIM values alone, however, are unable to determine whether the electron density arises from metal-metal bonding, (with accompanying orbital overlap), or simply owing to close metal centers due to crystal packing. To evaluate this, we turned to NLMO calculations (Table S10). No orbital interactions between the metal centers are observed for the **Eu1** and **Nd1** models as expected for lanthanide systems. In **Am1**; however, the NLMO analysis predicts an orbitalinteraction between the 5f shells of neighboring Am^{3+} metal centers (Figure 6), with mutual delocalization of unpaired electrons among the neighboring Am center. The NBO calculation classifies the interaction as an Am–Am bond. Although details about this interaction will need to be teased out by additional calculations, it seems noteworthy that the present density functional calculations identify a form of metal-metal covalency in **Am1**, but not the 4f analogs, which warrants further evaluation given the potential importance of these bonds in directing structural and spectroscopic properties.

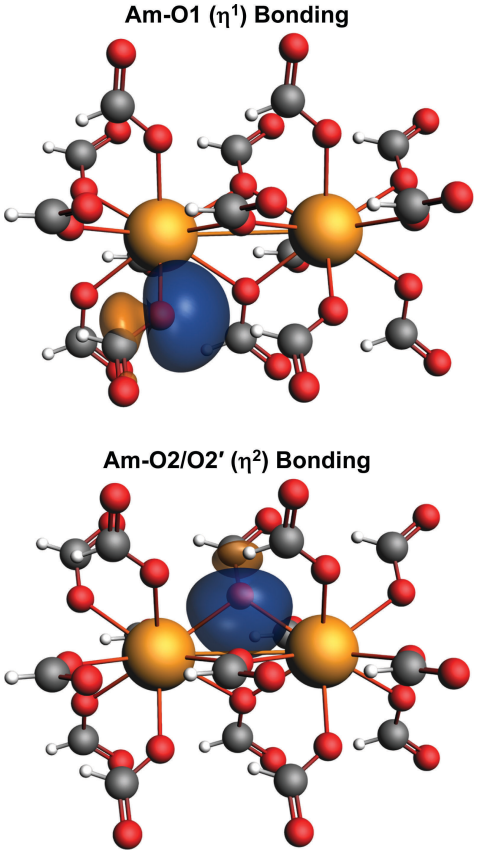

Figure 5. Representative NLMOs (+/–0.03 isosurfaces) calculated for **Am1** and representing inner sphere Am–O bonding.

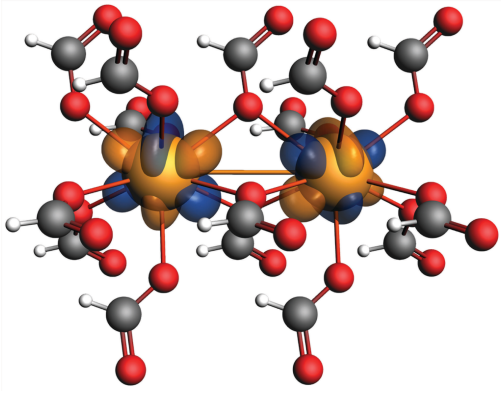

Figure 6. Representative Am–Am 2-center NLMO (+/– 0.03 isosurfaces) with 5f character calculated for **Am1**.

Optical Properties

UV-vis-NIR spectrum

Solid-state UV-vis-NIR diffuse reflectance spectroscopy was collected at room temperature on bulk microcrystalline material, Figure 7. The **Am1** spectra display Laporte forbidden *f-f* transitions typical of Am^{3+} bearing compounds. Two dominant bands are observed at 509 nm and 808 nm corresponding to transitions from the $^7F_{0'}$ ground state to the $^5L_{6'}$ and $^7F_{6'}$ excited states, respectively.[86,87] Weaker, less intense absorption bands are observed at wavelengths less than 475 nm and are attributed to a number of transitions from the $^7F_{0'}$ ground state to the higher energy states, such as $^5D_{2'}$ and $^5G_{2}$.[87,88] Overall, the **Am1** UV-vis-NIR absorption spectrum is rather unremarkable and similar to those of other Am^{3+} bearing materials as well as those obtained from solutions.[18,20,24,87–89] Extension of absorption measurements to **Eu1** and **Nd1** also reveal forbidden *f-f* transition typical for these lanthanide metals as reported elsewhere.[90–97]

Luminescence properties

To date only a few reported emissive Am^{3+} containing compounds are known from single crystals.[7,12,17,98,99] The compound **Am1** is an emissive material and as such. we have measured the luminescence spectrum, Figure 8. The excitation spectrum, when measured by monitoring at 703 nm, shows sharp bands at 510 nm, 423 nm, and 378 nm, all of which are characteristic of *f-f* transitions. When excited at 510 nm, **Am1** displays two narrow emission peaks at 596 nm and 703 nm. These bands result from direct excitation of the metal center and are *f-f* in origin and assigned to radiative decay from the $^5D_{1'}$ excited state to the $^7F_{0'}$ and $^7F_{1'}$ states, respectively.[100] In Am^{3+} materials the dominant emissive bands are observed at ~700 nm ($^7F_{1'}$) and ~825 nm ($^7F_{2'}$), however, in **Am1** the 596 nm ($^7F_{0'}$) emissive band is the most intense band.[7,12,17] Of the 12 known nine-coordinate Am^{3+} materials, this inversion of band intensity has never been observed.[1,2,21,4–6,12,13,15,17,20] This behavior was confirmed by collecting subsequent measurements on a second sample prepared via in situ routes (Figure S15).

Interpretation and rationalization of the Am^{3+} emission behavior was accomplished via comparison to **Eu1** and **Nd1** whose spectra are also shown in Figure 8. Primarily we are interested in the influence on optical properties from (1) the formate ligand and (2) metal site symmetry. Notably, a ligand-to-metal charge transfer band was not observed in the excitation spectrum of **Eu1** and **Nd1**. These bands are typically found in the high energy UV region (200 nm - 350 nm) and would be indicative of resonant energy transfer from the ligand to the metal. The absence of this excitation band demonstrates that for the compounds reported here, the ligands play a strictly structural role and do not electronically contribute to the optical behavior. Our early investigation into the structure of **Am1** led to two possible site symmetries (D_{3h} or C_{3v}) and is dependent on the extent of the difference between the Am–O2 and Am–O2′ bond lengths. These bond lengths, as described above, differ by only 0.23% making it unclear whether the difference is sufficient to reduce the overall symmetry from D_{3h} to C_{3v}. Analysis of the ^7F_j emission splitting in **Eu1** is particularly useful in differentiating symmetry. As has been well documented, splitting of Eu^{3+} emission bands are highly dependent on the metal site symmetry.[101–108] For those of D_{3h} symmetry, the $^5D_0 \rightarrow {}^7F_J$ transitions (J = 0-4) give rise to a splitting pattern of 0, 2, 1, 2, and 3 while for C_{3v} this pattern is 1, 2, 3, 3, and 5.[103,104] Close investigation of the **Eu1** emission profile, Figure S16, shows splitting of the ^7F_J emission consistent with C_{3v}, supporting our final symmetry assignment. This assignment separates **Am1** as the only nine coordinate Am^{3+} with C_{3v} symmetry for which emission is reported. Emission of seven-coordinate[17] (C_1), eight-coordinate[7,12,99] (C_1 and C_{2v}), and nine-coordinate[98] (C_1) are known and do not display a dominant $^5D_{1'} \rightarrow {}^7F_{0'}$ emission band. As such, we postulate that the peculiar optical behavior is a direct result of the unique symmetry of the metal site.

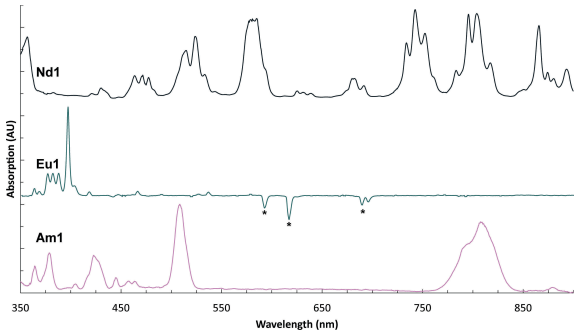

Figure 7. Solid-state diffuse reflectance spectra of **Am1**, **Eu1**, and **Nd1** collected at room temperature. Observed Eu^{3+} emission bands are denoted by (*).

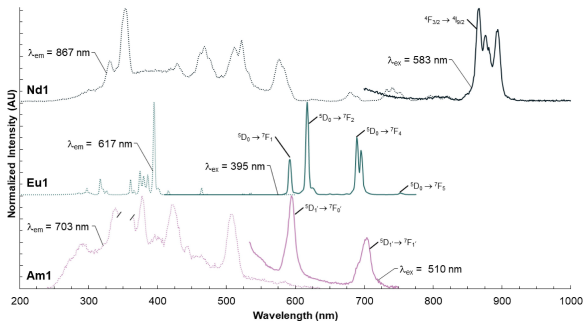

Figure 8. Luminescence spectra collected at 298 K on microcrystalline samples **of Am1**, **Eu1**, and **Nd1**. The excitation (dashed) and emission (solid) profiles and excitation wavelengths are provided. The break in the **Am1** spectra is due to the presence of a Rayleigh scattering peak.

Conclusions

The synthesis, structure, and optical properties of americium formate has been investigated to provide a baseline of comparison for future complex transuranium metal–organic frameworks and coordination polymers. Using the most basic of carboxylate linkers, the formate ions bridge Am^{3+} centers into a

3-D coordination polymer via η^1- and η^2 metal-oxygen bonding. The complex features a nine-coordinate metal center residing in a C_{3v} symmetry site, which is confirmed via the study of the Eu^{3+} and Nd^{3+} analogs. Infrared measurements with supporting QTAIM and NLMO calculations reveal that the Am–O bond is mostly ionic, but a secondary and important covalent component is present. The presence of orbital interactions between Am^{3+} centers is supported by theoretical findings and indicates participation of the 5f atomic orbitals. Luminescence spectra of the actinide compound collected at room temperature reveal two emission bands in the UV-vis region, which are assigned to decay from the $^5D_{1'}$ excited state to the $^7F_{1'}$ and $^7F_{0'}$ ground states. Notably, the $^7F_{0'}$ emission band is more intense than the $^7F_{1'}$ band and is an unreported behavior for americium-bearing compounds. With so few examples of complexes available, we postulate that the unusual behavior is a result of the unique symmetry environment. We are currently perusing the synthesis of new transuranium families that feature broad arrays of local symmetries and linker ligands to explore how these differences influence the actinide spectroscopic signatures.

Deposition Numbers 2161095, 2161094 contain the supplementary crystallographic data for this paper. These data are provided free of charge by the joint Cambridge Crystallographic Data Centre and Fachinformationszentrum Karlsruhe Access Structures service.

Acknowledgements

Work at PNNL was supported by the U.S. Department of Energy Office of Science, Office of Basic Energy Sciences, Division of Chemical Sciences, Geosciences and Biosciences, Heavy Element Chemistry program, FWP 73200. Work at the University of Buffalo was supported by the U.S. Department of Energy Office of Science, Office of Basic Energy Sciences, Division of Chemical Sciences, Geosciences and Biosciences, Heavy Element Chemistry program under award DESC0001136. L.C.D. acknowledges the National Laboratory for Scientific Computing (LNCC/MCTI, Brazil, SDumont supercomputer) and is grateful for support from São Paulo Research Foundation (FAPESP) #2017/17750-3 and CNPq #306844/2020-6 grants.

Conflict of Interests

The authors declare no conflict of interest.

Data Availability Statement

Data that support the findings of this study are available in the supplementary material of this article.

Keywords: americium · coordination polymers · metal-organic frameworks · photoluminescence · transuranic

[1] S. S. Galley, S. A. Pattenaude, C. A. Gaggioli, Y. Qiao, J. M. Sperling, M. Zeller, S. Pakhira, J. L. Mendoza-Cortes, E. J. Schelter, T. E. Albrecht-Schmitt, L. Gagliardi, S. C. Bart, *J. Am. Chem. Soc.* **2019**, *141*, 2356–2366.
[2] A. M. Fedosseev, M. S. Grigoriev, N. A. Budantseva, D. Guillaumont, C. Le Naour, É. Simoni, C. Den Auwer, P. Moisy, *Comptes Rendus Chim.* **2010**, *13*, 839–848.
[3] M. D. Danford, J. H. Burns, C. E. Higgins, J. R. Stokely, W. H. Baldwin, *Inorg. Chem.* **1970**, *9*, 1953–1955.
[4] F. Weigel, N. ter Meer, *Inorg. Nucl. Chem. Lett.* **1967**, *3*, 403–408.
[5] A. M. Fedoseev, M. N. Sokolova, M. S. Grigor'ev, N. A. Budantseva, *Radiochemistry* **2018**, *60*, 573–580.
[6] J. H. Burns, W. H. Baldwin, *Inorg. Chem.* **1977**, *16*, 289–294.
[7] J. N. Cross, J. A. Macor, J. A. Bertke, M. G. Ferrier, G. S. Girolami, S. A. Kozimor, J. R. Maassen, B. L. Scott, D. K. Shuh, B. W. Stein, S. C. E. Stieber, *Angew. Chem. Int. Ed.* **2016**, *55*, 12755–12759; *Angew. Chem.* **2016**, *128*, 12947–12951.
[8] J. H. Burns, M. D. Danford, *Inorg. Chem.* **1969**, *8*, 1780–1784.
[9] G. Andreev, N. Budantseva, A. Fedoseev, *Inorg. Chem. Commun.* **2019**, *99*, 160–163.
[10] S. K. Cary, J. Su, S. S. Galley, T. E. Albrecht-Schmitt, E. R. Batista, M. G. Ferrier, S. A. Kozimor, V. Mocko, B. L. Scott, C. E. Van Alstine, F. D. White, P. Yang, *Dalton Trans.* **2018**, *47*, 14452–14461.
[11] C. J. Windorff, C. Celis-Barros, J. M. Sperling, N. C. McKinnon, T. E. Albrecht-Schmitt, *Chem. Sci.* **2020**, *11*, 2770–2782.
[12] J. F. Corbey, B. M. Rapko, Z. Wang, B. K. McNamara, R. G. Surbella, K. L. Pellegrini, J. M. Schwantes, *Inorg. Chem.* **2018**, *57*, 2278–2287.
[13] S. K. Cary, M. Vasiliu, R. E. Baumbach, J. T. Stritzinger, T. D. Green, K. Diefenbach, J. N. Cross, K. L. Knappenberger, G. Liu, M. A. Silver, A. E. DePrince, M. J. Polinski, S. M. Van Cleve, J. H. House, N. Kikugawa, A. Gallagher, A. A. Arico, D. A. Dixon, T. E. Albrecht-Schmitt, *Nat. Commun.* **2015**, *6*, 6827.
[14] M. S. Grigoriev, A. M. Fedosseev, *Acta Crystallogr. Sect. C* **2011**, *67*, m205-m207.
[15] G. Tian, D. K. Shuh, C. M. Beavers, S. J. Teat, *Dalton Trans.* **2015**, *44*, 18469–18474.
[16] A. M. Fedosseev, A. V. Gogolev, I. A. Charushnikova, V. P. Shilov, *Radiochim. Acta* **2011**, *99*, 679–686.
[17] J. A. Ridenour, R. G. Surbella, A. V. Gelis, D. Koury, F. Poineau, K. R. Czerwinski, C. L. Cahill, *Angew. Chem. Int. Ed.* **2019**, *58*, 16508–16511; *Angew. Chem.* **2019**, *131*, 16660–16663.
[18] F. D. White, A. N. Gaiser, E. J. Warzecha, J. M. Sperling, C. Celis-Barros, S. R. Salpage, Y. Zhou, T. Dilbeck, A. J. Bretton, D. S. Meeker, K. G. Hanson, T. E. Albrecht-Schmitt, *Inorg. Chem.* **2018**, *57*, 12969–12975.
[19] N. Brenner, J. M. Sperling, T. N. Poe, C. Celis-Barros, K. Brittain, E. M. Villa, T. E. Albrecht-Schmitt, M. J. Polinski, *Inorg. Chem.* **2020**, *59*, 9384–9395.
[20] D. Dan, C. Celis-Barros, F. D. White, J. M. Sperling, T. E. Albrecht-Schmitt, *Chem. Eur. J.* **2019**, *25*, 3248–3252.
[21] A. V. Gogolev, M. S. Grigoriev, N. A. Budantseva, A. M. Fedosseev, *Russ. J. Coord. Chem.* **2013**, *39*, 271–277.
[22] A. B. Yusov, M. S. Grigor'ev, A. M. Fedoseev, P. Moisy, V. P. Shilov, A. V. Gogolev, *Radiochemistry* **2015**, *57*, 6–19.
[23] N. A. Budantseva, M. S. Grigoriev, A. M. Fedosseev, *Radiochim. Acta* **2014**, *102*, 377–384.
[24] J. N. Cross, J. Su, E. R. Batista, S. K. Cary, W. J. Evans, S. A. Kozimor, V. Mocko, B. L. Scott, B. W. Stein, C. J. Windorff, P. Yang, *J. Am. Chem. Soc.* **2017**, *139*, 8667–8677.
[25] S. S. Galley, J. M. Sperling, C. J. Windorff, M. Zeller, T. E. Albrecht-Schmitt, S. C. Bart, *Organometallics* **2019**, *38*, 606–609.
[26] R. E. Wilson, T. J. Carter, M. Autillo, S. Stegman, *Chem. Commun.* **2020**, *56*, 2622–2625.
[27] P. Lindqvist-Reis, C. Apostolidis, J. Rebizant, A. Morgenstern, R. Klenze, O. Walter, T. Fanghänel, R. G. Haire, *Angew. Chem. Int. Ed.* **2007**, *46*, 919–922; *Angew. Chem.* **2007**, *119*, 937–940.
[28] C. A. P. Goodwin, J. Su, T. E. Albrecht-Schmitt, A. V. Blake, E. R. Batista, S. R. Daly, S. Dehnen, W. J. Evans, A. J. Gaunt, S. A. Kozimor, N. Lichtenberger, B. L. Scott, P. Yang, *Angew. Chem. Int. Ed.* **2019**, *58*, 11695–11699; *Angew. Chem.* **2019**, *131*, 11821–11825.
[29] I. A. Charushnikova, A. M. Fedoseev, V. P. Perminov, *Radiochemistry* **2015**, *57*, 111–121.
[30] C. Tamain, B. Arab-Chapelet, M. Rivenet, X. F. Legoff, G. Loubert, S. Grandjean, F. Abraham, *Inorg. Chem.* **2016**, *55*, 51–61.
[31] L. H. Jones, *J. Chem. Phys.* **1955**, *23*, 2105–2107.
[32] K. Lv, S. Fichter, M. Gu, J. März, M. Schmidt, *Coord. Chem. Rev.* **2021**, *446*, 214011.

[33] A. M. Hastings, M. Fairley, M. C. Wasson, D. Campisi, A. Sarkar, Z. C. Emory, K. Brunson, D. B. Fast, T. Islamoglu, M. Nyman, P. C. Burns, L. Gagliardi, O. K. Farha, A. E. Hixon, J. A. LaVerne, *Chem. Mater.* **2022**, *34*, 8403–8417.
[34] A. M. Hastings, D. Ray, W. Jeong, L. Gagliardi, O. K. Farha, A. E. Hixon, *J. Am. Chem. Soc.* **2020**, *142*, 9363–9371.
[35] N. P. Martin, J. März, H. Feuchter, S. Duval, P. Roussel, N. Henry, A. Ikeda-Ohno, T. Loiseau, C. Volkringer, *Chem. Commun.* **2018**, *54*, 6979–6982.
[36] S. E. Gilson, P. Li, J. E. S. Szymanowski, J. White, D. Ray, L. Gagliardi, O. K. Farha, P. C. Burns, *J. Am. Chem. Soc.* **2019**, *141*, 11842–11846.
[37] E. C. Spencer, J. Zhao, N. L. Ross, M. B. Andrews, R. G. Surbella, C. L. Cahill, *J. Solid State Chem.* **2013**, *202*, 99–104.
[38] D. T. de Lill, N. S. Gunning, C. L. Cahill, *Inorg. Chem.* **2005**, *44*, 258–266.
[39] H.-C. Zhou, J. R. Long, O. M. Yaghi, *Chem. Rev.* **2012**, *112*, 673–674.
[40] A. E. Baumann, D. A. Burns, B. Liu, V. S. Thoi, *Commun. Chem.* **2019**, *2*, 86.
[41] M. Safaei, M. M. Foroughi, N. Ebrahimpoor, S. Jahani, A. Omidi, M. Khatami, *TrAC Trends Anal. Chem.* **2019**, *118*, 401–425.
[42] G. H. Morritt, H. Michaels, M. Freitag, *Chem. Phys. Rev.* **2022**, *3*, 011306.
[43] W. L. Leong, J. J. Vittal, *Chem. Rev.* **2011**, *111*, 688–764.
[44] R. Bolotovsky, A. Bulkin, G. Krutov, V. Kudryashev, V. Trunov, V. Ul'yanov, O. Antson, P. Hiismäki, H. Pöyry, A. Tiitta, A. Loshmanov, N. Furmanova, *Solid State Commun.* **1990**, *76*, 1045–1049.
[45] P. Kistaiah, K. Sathyanarayana Murthy, L. Iyengar, K. V. Krishna Rao, *J. Mater. Sci.* **1981**, *16*, 2321–2323.
[46] G. Lorusso, J. W. Sharples, E. Palacios, O. Roubeau, E. K. Brechin, R. Sessoli, A. Rossin, F. Tuna, E. J. L. McInnes, D. Collison, M. Evangelisti, *Adv. Mater.* **2013**, *25*, 4653–4656.
[47] J.-M. Lin, Y.-F. Guan, D.-Y. Wang, W. Dong, X.-T. Wang, S. Gao, *Dalton Trans.* **2008**, 6165.
[48] S. Deng, N. Zhang, W. Xiao, C. Chen, *Zeitschrift für Krist. – New Cryst. Struct.* **2009**, *224*, 275–276.
[49] Y. Xu, S.-H. Ding, G.-P. Zhou, Y.-G. Liu, *Acta Crystallogr. Sect. E* **2006**, *62*, m1749-m1750.
[50] Y. B. Go, A. J. Jacobson, *Chem. Mater.* **2007**, *19*, 4702–4709.
[51] M. Song, Y. Dang, J. Dong, X. Zhang, S. Lei, W. Hu, *Nanoscale* **2019**, *11*, 21061–21067.
[52] A. Chadha, S. Sampath, D. M. Chackraburtty, *Inorg. Chim. Acta* **1980**, *42*, 163–167.
[53] M. Liu, Z. Li, J. Xiong, Y. Jiang, T. Tang, J. Qiu, J. Yao, S. W. Ng, C. Zeng, *J. Rare Earth* **2021**, *39*, 1194–1203.
[54] I. Mayer, M. Steinberg, F. Feigenblatt, A. Glasner, *J. Phys. Chem.* **1962**, *66*, 1737–1738.
[55] C. Hennig, A. Ikeda-Ohno, W. Kraus, S. Weiss, P. Pattison, H. Emerich, P. M. Abdala, A. C. Scheinost, *Inorg. Chem.* **2013**, *52*, 11734–11743.
[56] SAINT Version 8.34a, **2013**.
[57] G. M. Sheldrick, **2005**.
[58] Bruker Nano, **2019**.
[59] L. J. Farrugia, *J. Appl. Crystallogr.* **2012**, *45*, 849–854.
[60] M. N. Burnett, C. K. Johnson, *ORTEP-III: Oak Ridge Thermal Ellipsoid Plot Program for Crystal Structure Illustrations*, Oak Ridge National Laboratory Report ORNL-6895, **1996**.
[61] D. E. Newbury, N. W. M. Ritchie, *J. Mater. Sci.* **2015**, *50*, 493–518.
[62] G. te Velde, F. M. Bickelhaupt, E. J. Baerends, C. Fonseca Guerra, S. J. A. van Gisbergen, J. G. Snijders, T. Ziegler, *J. Comput. Chem.* **2001**, *22*, 931–967.
[63] E. D. Glendening, C. R. Landis, F. Weinhold, *J. Comput. Chem.* **2013**, *34*, 1429–1437.
[64] R. Brown, A. Bennet, H. Slebocka-Tilk, *Acc.Chem.Res.* **1992**, *25*, 481–588.
[65] R. D. Shannon, *Acta Crystallogr. Sect. A* **1976**, *32*, 751–767.
[66] J. N. Cross, E. M. Villa, S. Wang, J. Diwu, M. J. Polinski, T. E. Albrecht-Schmitt, *Inorg. Chem.* **2012**, *51*, 8419–8424.
[67] K. Ito, H. J. Bernstein, *Can. J. Chem.* **1956**, *34*, 170–178.
[68] S. Alvarez, *Dalton Trans.* **2013**, *42*, 8617.
[69] A. Álvarez, M. Borges, J. J. Corral-Pérez, J. G. Olcina, L. Hu, D. Cornu, R. Huang, D. Stoian, A. Urakawa, *ChemPhysChem* **2017**, *18*, 3135–3141.
[70] D. Koch, Y. Chen, P. Golub, S. Manzhos, *Phys. Chem. Chem. Phys.* **2019**, *21*, 20814–20821.
[71] C. D. Montgomery, *J. Chem. Educ.* **2007**, *84*, 102.
[72] C. F. Matta, R. J. Boyd, in *Quantum Theory Atoms Mol.*, Wiley-VCH Verlag GmbH & Co. KGaA, Weinheim, Germany, **n.d.**, pp. 1–34.
[73] X. Yu, D.-C. Sergentu, R. Feng, J. Autschbach, *Inorg. Chem.* **2021**, *60*, 17744–17757.
[74] J. Dominikowska, M. Palusiak, *Struct. Chem.* **2012**, *23*, 1173–1183.
[75] J. P. Tidey, V. V. Zhurov, C. G. Gianopoulos, T. S. Hermann, A. A. Pinkerton, *J. Phys. Chem. A* **2018**, *122*, 9676–9687.
[76] D. B. McWhan, B. B. Cunningham, J. C. Wallmann, *J. Inorg. Nucl. Chem.* **1962**, *24*, 1025–1038.
[77] S. M. Ciborowski, A. Mitra, R. M. Harris, G. Liu, P. Sharma, N. Khetrapal, M. Blankenhorn, L. Gagliardi, K. H. Bowen, *J. Am. Chem. Soc.* **2021**, *143*, 17023–17028.
[78] H.-S. Hu, N. Kaltsoyannis, *Phys. Chem. Chem. Phys.* **2017**, *19*, 5070–5076.
[79] B. O. Roos, P.-Å. Malmqvist, L. Gagliardi, *J. Am. Chem. Soc.* **2006**, *128*, 17000–17006.
[80] G. Cavigliasso, N. Kaltsoyannis, *Inorg. Chem.* **2006**, *45*, 6828–6839.
[81] A. Jaroš, C. Foroutan-Nejad, M. Straka, *Inorg. Chem.* **2020**, *59*, 12608–12615.
[82] A. Chandrasekar, T. K. Ghanty, *Inorg. Chem.* **2019**, *58*, 3744–3753.
[83] X. Zhang, Y. Wang, R. Morales-Martínez, J. Zhong, C. de Graaf, A. Rodríguez-Fortea, J. M. Poblet, L. Echegoyen, L. Feng, N. Chen, *J. Am. Chem. Soc.* **2018**, *140*, 3907–3915.
[84] J. T. Boronski, J. A. Seed, D. Hunger, A. W. Woodward, J. van Slageren, A. J. Wooles, L. S. Natrajan, N. Kaltsoyannis, S. T. Liddle, *Nature* **2021**, *598*, 72–75.
[85] N. Castillo, C. F. Matta, R. J. Boyd, *Chem. Phys. Lett.* **2005**, *409*, 265–269.
[86] P. R. Zalupski, T. S. Grimes, C. R. Heathman, D. R. Peterman, *Appl. Spectrosc.* **2017**, *71*, 2608–2615.
[87] R. Pappalardo, W. T. Carnall, P. R. Fields, *J. Chem. Phys.* **1969**, *51*, 842–843.
[88] W. T. Carnall, B. G. Wybourne, *J. Chem. Phys.* **1964**, *40*, 3428–3433.
[89] S. E. Stephanou, J. P. Nigon, R. A. Penneman, *J. Chem. Phys.* **1953**, *21*, 42–45.
[90] K. Binnemans, C. Görller-Walrand, *J. Alloys Compd.* **1997**, *250*, 326–331.
[91] P. K. Gallagher, *J. Chem. Phys.* **1964**, *41*, 3061–3069.
[92] W. T. Carnall, P. R. Fields, K. Rajnak, *J. Chem. Phys.* **1968**, *49*, 4412–4423.
[93] W. T. Carnall, P. R. Fields, B. G. Wybourne, *J. Chem. Phys.* **1965**, *42*, 3797–3806.
[94] W. T. Carnall, P. R. Fields, K. Rajnak, *J. Chem. Phys.* **1968**, *49*, 4424–4442.
[95] E. Y. Wong, *J. Chem. Phys.* **1961**, *34*, 1989–1993.
[96] E. H. Carlson, G. H. Dieke, *J. Chem. Phys.* **1961**, *34*, 1602–1609.
[97] A. A. Migdisov, A. Williams-Jones, *Geochim. Cosmochim. Acta* **2002**, *66*, 4311–4323.
[98] A. Arteaga, A. D. Nicholas, L. C. Ducati, J. Autschbach, R. G. Surbella, *Inorg. Chem.* **2023**, DOI 10.1021/acs.inorgchem.2c03976.
[99] R. D. M. Greer, C. Celis-Barros, J. M. Sperling, A. N. Gaiser, C. J. Windorff, T. E. Albrecht-Schönzart, *Inorg. Chem.* **2020**, *59*, 16291–16300.
[100] P. Thouvenot, S. Hubert, C. Moulin, P. Decambox, P. Mauchien, *ract* **1993**, *61*, 15–22.
[101] N. M. Shavaleev, S. V. Eliseeva, R. Scopelliti, J.-C. G. Bünzli, *Inorg. Chem.* **2015**, *54*, 9166–9173.
[102] S. Yamauchi, T. Hashibe, M. Murase, H. Hagiwara, N. Matsumoto, M. Tsuchimoto, *Polyhedron* **2013**, *49*, 105–112.
[103] P. A. Tanner, *Chem. Soc. Rev.* **2013**, *42*, 5090.
[104] K. Binnemans, *Coord. Chem. Rev.* **2015**, *295*, 1–45.
[105] N. M. Shavaleev, S. V. Eliseeva, R. Scopelliti, J.-C. G. Bünzli, *Inorg. Chem.* **2010**, *49*, 3927–3936.
[106] D. Parker, E. A. Suturina, I. Kuprov, N. F. Chilton, *Acc. Chem. Res.* **2020**, *53*, 1520–1534.
[107] A. C. Harnden, E. A. Suturina, A. S. Batsanov, P. K. Senanayake, M. A. Fox, K. Mason, M. Vonci, E. J. L. McInnes, N. F. Chilton, D. Parker, *Angew. Chem.* **2019**, *131*, 10396–10400; *Angew. Chem. Int. Ed.* **2019**, *58*, 10290–10294.
[108] K. Binnemans, C. Görller-Walrand, *Chem. Phys. Lett.* **1995**, *245*, 75–78.

Manuscript received: January 9, 2023
Accepted manuscript online: March 27, 2023
Version of record online: June 13, 2023